International Journal of Nanomedicine

Dovepress
open access to scientific and medical research

Open Access Full Text Article

ORIGINAL RESEARCH

Intestinal Targeted Nanogel with Broad-Spectrum Autonomous ROS Scavenging Performance for Enhancing the Bioactivity of *trans*-Resveratrol

Jingwen Xu[1,2], Yue Zhang[1,2], Xiaolin Yao[1], Sijuan Wang[1,2], Kaiqiang Lv[1,2], Guangwen Luo[1,2], Jiaqi Wang[1,2], Guoliang Li[1]

[1]School of Food Science and Engineering, School of Biological and Pharmaceutical Sciences, Shaanxi University of Science & Technology, Xi'an, 710021, People's Republic of China; [2]Xi'an Key Laboratory of Antiviral and Antimicrobial-Resistant Bacteria Therapeutics Research, Xi'an, 710021, People's Republic of China

Correspondence: Guoliang Li, Email 61254368@163.com

Introduction: To improve the bioavailability of *trans*-resveratrol (*trans*-Res), it is commonly co-delivered with antioxidant bioactives using a complex synthetic intestinal targeted carrier, however, which makes practical application challenging.

Methods: A nanogel (Ngel), as broad-spectrum autonomous ROS scavenger, was prepared using selenized thiolated sodium alginate (TSA-Se) and crosslinked with calcium lactate (CL) for loading *trans*-Res to obtain Ngel@Res, which maintained spherical morphology in the upper digestive tract but broke down in the lower digestive tract, resulting in *trans*-Res release.

Results: Under protection of Ngel, *trans*-Res showed enhanced stability and broad-spectrum ROS scavenging activity. The synergistic mucoadhesion of Ngel prolonged the retention time of *trans*-Res in the intestine. Ngel and Ngel@Res increased the lifespan of *Caenorhabditis elegans* to 26.00 ± 2.17 and 26.00 ± 4.27 days by enhancing the activity of antioxidases, upregulating the expression of *daf-16, sod-5* and *skn-1*, while downregulating the expression of *daf-2* and *age-1*.

Conclusion: This readily available, intestinal targeted selenized alginate-based nanogel effectively improves the bioactivity of *trans*-Res.

Keywords: *trans*-resveratrol, seleno-alginate, synergistic antioxidant, mucoadhesion, intestinal targeted delivery

Introduction

The growing emphasis on wellness has led to a significant interest in nutraceuticals and cosmetics containing bioactives.[1] A particular bioactive, 3,4',5-*trans*-trihydroxystilbene (*trans*-resveratrol, abbreviated as *trans*-Res) has garnered considerable attention due to its various beneficial properties such as anticancer, antioxidant, anti-inflammatory, anti-aging and cardiovascular protection.[2] Res, a natural occurring stilbene, is a phytoalexin that is synthesized in large quantities when plants like grapes, peanuts, and berries are exposed to external stimuli.[3,4] However, the wide applications of *trans*-Res are hindered by its low bioavailability caused by poor water-solubility and vulnerability to isomeric conversion and rapid degradation when *trans*-Res in various harsh environments.[5–8] Although oral absorption of *trans*-Res can reach up to 75%, only trace amounts of *trans*-Res are detectable in blood.[9] In addition, *trans*-Res only shows 2,2-diphenyl-1-picrylhydrazyl (DPPH) and 2, 2'-azino-bis(3-ethylbenzothiazoline-6-sulfonic acid) ($ABTS^{+}$) radical scavenging effects.[10] The representative strategy to enhance the limited antioxidant property of *trans*-Res is by co-delivering of *trans*-Res with other antioxidants. However, some organic reagents and complex modification procedures are inevitably involved during the preparation of the carrier,[11–13] following the co-encapsulation of *trans*-Res and other antioxidants. This tactic is not only complex, but also difficult to elucidate its synergistic mechanism.

To date, various delivery systems such as liposomes, exosomes, nanoemulsion, nanogel (a polymer-based, crosslinked hydrogel particle on the sub-micron scale), nanofiber, nanocrystal, nanosphere and nanomicelles composed of biomacromolecules have been prepared in recent years for the codelivery of *trans*-Res and other antioxidants.[14] Particularly, with the

Received: 19 February 2024
Accepted: 4 June 2024
Published: 14 June 2024

Graphical Abstract

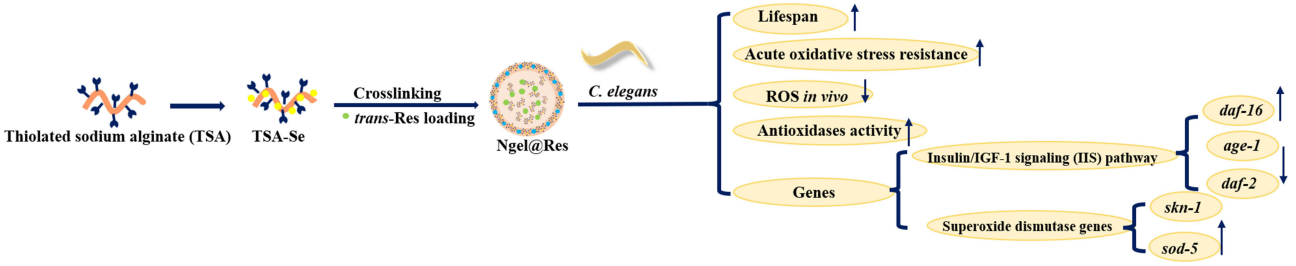

introduction of nanotechnology, the unprecedented advantages of food-borne polysaccharides have been revealed in protecting, loading, transporting and controlling the release of bioactives by responding to various physiological signals like pH, enzymes, temperature, etc.[15] For instance, sodium alginate (SA), a natural polysaccharide containing α-L-guluronic acid (G block) and β-D-mannuronic acid (M block), can be crosslinked by Ca^{2+} to form "egg box structure".[16,17] The resulting calcium alginate layer is not degraded in the upper digestive tract but is digested by beneficial bacteria when it reaches the lower digestive tract.[18,19] In view of the structural feature of the 'stomach fold' and "intestine break", calcium alginate is commonly used for intestinal targeted delivery of bioactive component.[20,21] To achieve precise intestinal targeting, formation of disulfide bonds between carriers containing thiol groups and the mucin with a large number of thiol groups is a widely used tactic.[22,23] To this aim, some thiol-contained carriers such as SA and β-cyclodextrin (CD) have been developed. However, it was found that gastric mucoadhesion occurred before intestinal mucoadhesion, which hindered the improvement of bioavailability of the payloads.[22,24]

Among the many antioxidant substances, selenium (Se) is an essential trace element with several physiological activities, including antioxidant, anti-aging, anti-inflammatory, anticancer, and damaged cell repair, as well as improvement of immunomodulatory function.[25] Li et al discovered that selenium deficiency could cause the imbalance of selenium protein content, oxidative stress, inflammation and apoptosis, leading to spleen injury.[26] Although Se nanoparticles (Se NPs) have a great potential in daily diets as its higher bioavailability and lower toxicity compared with chemogenic Se, the instability and tendency to aggregate still pose noticeable challenges for practical applications. Fortunately, natural polysaccharides can reduce surface energy and prevent aggregation through hydrogen bonding and electrostatic interactions. Seleno-polysaccharides, a type of organic selenium materials, are more preferable as dietary supplements for long-term use as their excellent biosafety, biostability, and ease of absorption.[27,28]

Herein, we proposed a green and convenient strategy to enhance the bioactivity of *trans*-Res by utilizing a selenized alginate-based intestinal targeted nanogel with broad-spectrum ROS autonomous scavenging performance. Firstly, a calcium lactate (CL) crosslinked selenized thiolated SA (referred to as TSA-Se/CL and abbreviated as Ngel thereinafter) was prepared for the intestinal targeted delivery of *trans*-Res. The chemical structure of Ngel and *trans*-Res loaded Ngel (named as Ngel@Res) was characterized using H nuclear magnetic resonance (^{1}H NMR), Fourier transform infrared spectroscopy (FTIR) and X-Ray Diffraction (XRD), etc. The loading capacity of Ngel for *trans*-Res was also assessed. Furthermore, we evaluated the effect of Ngel on the ROS scavenging behavior of *trans*-Res before and after digestion to elucidate their synergistic free radical scavenging mechanism. The effect of Ngel on the pH, temperature, ultraviolet and redox resistance of *trans*-Res was investigated. The intestinal targeting mechanism of Ngel was explored through mucoadhesive ability and in vitro release behavior. Finally, the mechanism of prolonging the lifespan of *Caenorhabditis elegans* (*C. elegans*) was revealed (Figure 1A). This work is expected to provide theoretical basis for anti-aging investigation.

Experimental Section

Materials and Reagents

Trans-resveratrol (*trans*-Res, 99%), sodium alginate (SA, viscosity 200 ± 20 mpa·s) were provided by Shanghai Aladdin Biochemical Technology Co. Ltd. Mercaptoacetic acid (MTA, 99%), ascorbic acid (AsA, 99%), pepsin from pig (1:3000,

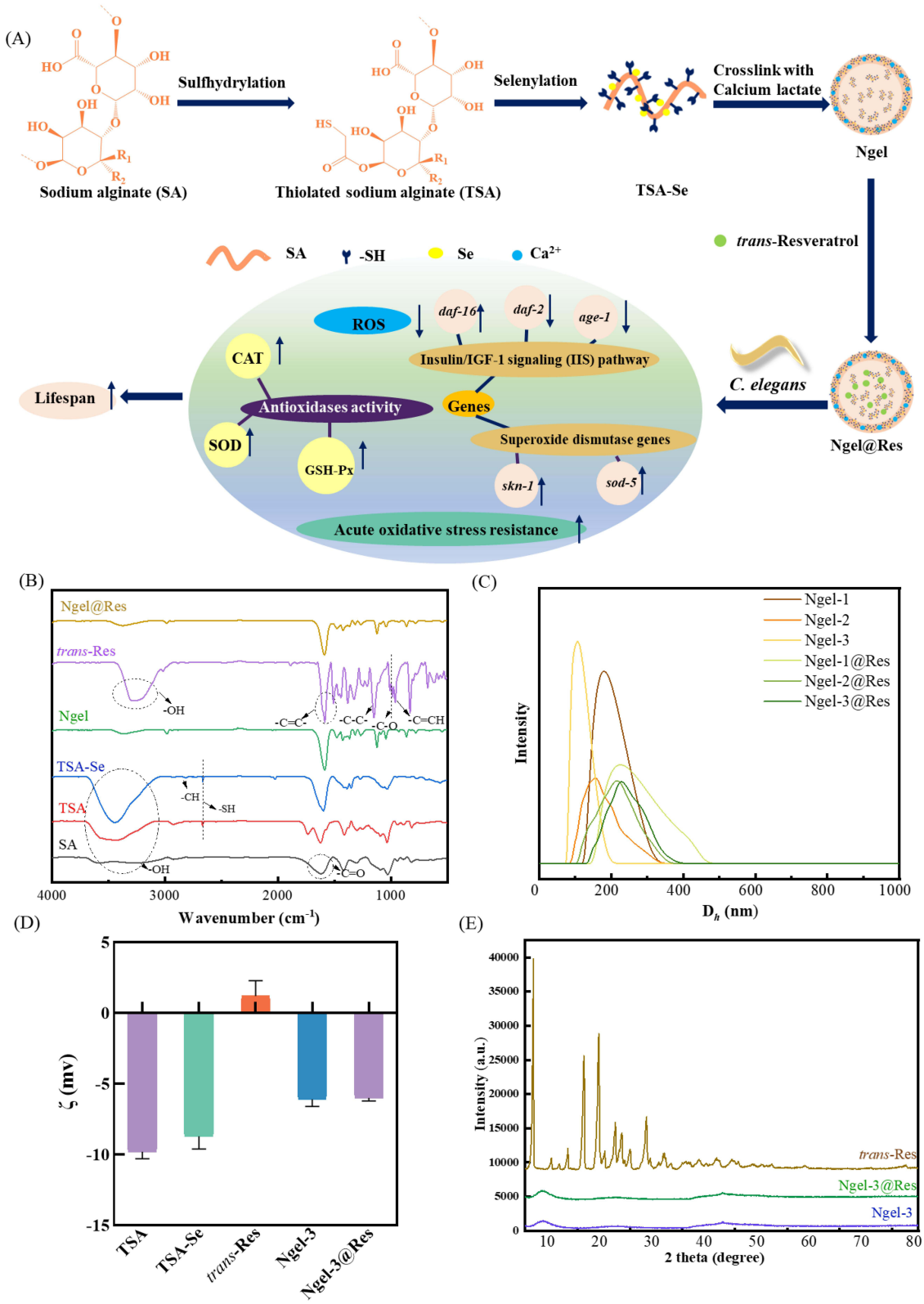

Figure 1 (**A**) Synthesis of TSA and TSA-Se, formation of Ngel, *trans*-Res loaded Ngel (Ngel@Res) and its anti-aging mechanism for *C. elegans*. (**B**) FTIR spectra of Ngel and its precursors, as well as Ngel@Res. (**C**) D_h of the Ngel and Ngel@Res nanogels with different compositions. (**D**) Zeta potentials of TSA, TSA-Se, *trans*-Res, Ngel-3 and Ngel-3@Res. (**E**) XRD patterns of *trans*-Res, Ngel-3 and Ngel-3@Res.

>3000 U/mg), trypsin from pig (1:250), bile salt from pig (BR), α-Amylase from *Aspergillus oryzae* (40,000 U/g), 2',7'-dichlorodihydrofluorescein diacetate (DCFH-DA, 97%, 50 μM) and levamisole (99%, 60 μM) were offered by Shanghai Macklin Biochemical Co., Ltd. Unless otherwise specified, all reagents are provided by commercial suppliers.

Synthesis of Ngel and Ngel@Res

Synthesis of Thiolated SA (TSA)

TSA was synthesized using the method reported by Khalid et al.[24] Typically, SA (1 g) was dissolved in 30 mL deionized (DI) water, then 1.125 mL MTA was added, following the addition of 1 mL HCl (7M) for acidification. The reaction was performed at 80 °C for 3 h. At the end of this reaction, the mixture was precipitated in excess ether to remove the unbounded MTA. The collected precipitation was freeze-dried for 24 h, the resulting white solid was TSA (Yield: 52.7%). The content of -SH group in TSA was determined by Ellman's experiment, the experimental procedure was described in Supporting Information Item S1.

Selenization of TSA

TSA aqueous solution (0.3 w/v, 3.5 mL) and 0.4 mL AsA aqueous solution with different concentrations (50, 75, 100 mM) were mixed, respectively. Then, 0.1 mL Na_2SeO_3 with the same concentration was added to each mixture under stirring for 12 h. The resulting mixture was transferred into dialysis tube (Molecular weight cut-off: 3500 Da) and immersed in DI water for the removal of superfluous AsA. The water out of the tube was replaced at specific time intervals. Afterward, the dialysate was collected and lyophilized, yielding selenized TSA with different Se contents, which were abbreviated as TSA-Se-1, TSA-Se-2 and TSA-Se-3 in the same order as Se concentration.

Synthesis of Nanogels

TSA-Se (1 mg) was completely dissolved in DI water (1 mL) and mixed with an ethanol solution containing *trans*-Res (0.4 mL, 6 mg mL^{-1}) with stirring overnight. The resulting mixed solution was then added dropwise into 6 mL calcium lactate (CL, 1% w/v) solution with stirring. After 1 h, the mixture was centrifuged at 3000 rpm for 3 min, and the supernatant was collected for freeze-drying to prepare the *trans*-Res loaded nanogels, abbreviated as Ngel-1@Res, Ngel-2@Res, and Ngel-3@Res, according to the order of selenium content from 50 to 100 mM. Similarly, an aqueous solution (1.4 mL) containing TSA-Se (1 mg) was crosslinked using CL solution with stirring to prepare blank nanogels, named as Ngel-1, Ngel-2 and Ngel-3.

Instruments and Characterization

The chemical structure of nanogels and their precursors were characterized by ^1H NMR (600 MHz, nuclear magnetic resonance spectrometer, Bruker AVANCE, Germany) and FTIR (Fourier infrared spectrometer VECTOR-22, Bruker, Germany) at 25°C, respectively. D_2O was used as the solvent, and tetramethylsilane as the internal standard, respectively. FTIR spectra ranging from 4000 to 400 cm^{-1} were obtained using the KBr pellets technique. The diffraction patterns were measured using X-ray powder diffraction (XRD, Malvern Panalytical) under the following conditions: 0.03° step size, 0.5 s step time, and 2 theta ranging 5°~80°. The hydrodynamic diameter (D_h) and its corresponding polydispersity index (PDI), along with the Zeta potential (ζ) of the nanogels were measured using the Zeta Potential Nano-size analyzer (Anton Paar, Austria) at a contact angle of 90° and 25 °C. The morphological changes of the nanogels were observed using transmission electron microscopy (TEM, FEI Tecnai G2 F20 S-TWIN, FEI, America). For sample preparation, an aqueous solution of nanogels (10 μL, 500 μg mL^{-1}) was dropwise added onto a copper grid (200 mesh) and air-dried. The following observation was conducted at an accelerating voltage of 200 kV in TEM. Energy Dispersive X-ray Spectroscopy (EDS) maps were acquired on an EDS detectors (FEI, SuperX). The Field Emission Gun (FEG) electron source was operated at an acceleration voltage of 200 KV.

Trans-Res Loading Behavior

Determination of Calibration Curve of *Trans*-Res

Trans-Res was dissolved in 50 wt% aqueous ethanol to prepare the solution with the concentration of 2–30 μg mL^{-1}. The calibration curve of *trans*-Res was established by measuring the absorbance (A) of the standard solution at 305 nm and its corresponding concentration (C) as follows:

$$C\left(\mu g\ mL^{-1}\right) = \frac{A - 0.13043}{0.07129}\left(R^2 = 0.9998\right) \quad (1)$$

Calculation of Loading Content (LC) and Encapsulation Efficiency (EE)

The LC and EE were evaluated by ultrasonic grinding approach. Briefly, Ngel@Res powder (5 mg) was ground using a mortar and dissolved in DI water to reach the concentration of 0.5 mg mL^{-1}. The solution was then subjected to ultrasonication at 40 W for 30 min to destroy the structure of Ngel@Res. The resulting solution was diluted with isomeric ethanol and the UV–vis absorbance was measured at 305 nm. The LC and EE of *trans*-Res were calculated in line with the following equation:

$$LC\,(\%) = \frac{mass\ of\ trans - Res\ in\ Ngel@Res}{mass\ of\ Ngel@Res} \times 100\% \quad (2)$$

$$EE\,(\%) = \frac{mass\ of\ trans - Res\ in\ Ngel@Res}{mass\ of\ trans - Res\ added\ initiallly} \times 100\% \quad (3)$$

Stability of Ngel@Res

pH

The Ngel@Res and *trans*-Res were dissolved in PBS at pH 2.0, 5.0 and 7.0 PBS, with the concentration of 3 mg mL^{-1}, and incubated at 37 °C for 5 h, respectively.

Temperature

The Ngel@Res and *trans*-Res were dissolved in DI water at a concentration of 3 mg mL^{-1} and stored at 25, 37 and 60 °C for 5 h, respectively.

Redox

To assess the Redox resistance of *trans*-Res, 1.0% (v/v) H_2O_2 and 0.20% (w/v) Na_2SO_3 were used as oxidant and reductant, respectively. Ngel and *trans*-Res were dissolved in 1.0% (v/v) H_2O_2 and 0.20% (w/v) Na_2SO_3 at a concentration of 3 mg mL^{-1}, and stored for 5 h.

Ultraviolet

The Ngel@Res and *trans*-Res were dissolved in DI water at a concentration of 3 mg mL^{-1} and exposed on intermittent Ultraviolet radiation from an ultraviolet lamp (Shenglan, ZF-6) at 1 mW cm^{-2} for 5 h.

At predetermined time intervals, the retention rate of *trans*-Res with and without the aid of Ngel was evaluated using equation (4). All experiments were performed thrice.

$$Retention\ rate\,(\%) = \frac{the\ surplus\ amount\ of\ trans - Res\ after\ treatment}{the\ total\ amount\ of\ trans - Res} \times 100\% \quad (4)$$

ROS Scavenging Efficacy

The ROS scavenging efficiency of Ngel was investigated before and after digestion using simulated gastrointestinal fluids. Initially, 80 mg Ngel@Res powder was suspended in 40 mL SGF (pepsin 0.32%, NaCl 0.20%, pH=2.0) and incubated at 37 °C with stirring, after 2 h, the Ngel@Res was collected and freeze-dried. Subsequently, the pH of the mixture was then adjusted to 7.0 with 0.68% (w/v) potassium dihydrogen phosphate, an equal portion of 0.32% (w/v) trypsin and NaOH. The

mixture was incubated at 37°C for 4 h, the samples were collected and lyophilized. •DPPH, •$ABTS^+$, •OH were selected to assess the ROS scavenging efficacy of the nanogels. Free *trans*-Res and AsA were regarded as control groups.

OH• Clearance Test

The scavenging effect of the samples on •OH radicals was investigated using the Fenton reaction photochemical method.[29] The mechanism for measuring the •OH radical scavenging ability is that salicylic acid can capture the •OH produced from the Fenton reaction and resulting in the formation of colored substances with absorption at 510 nm.[30] When the nanogels with antioxidant properties are added, they can capture •OH and reduce the production of colored substances, which can be measured by UV absorption. A lower absorbance indicates a higher •OH scavenging rate and a more powerful antioxidant property.[31] The experimental setup includes homogenously mixing $FeSO_4$ (50 μL, 9 mM), an ethanol solution containing salicylic acid (50 μL, 9 mM), and the sample (50 μL). Then, H_2O_2 (50 μL, 8.8 mM) was added to trigger the reaction. After incubation at 37°C for 30 min, the UV–vis absorption at 510 nm was measured. AsA and DI water were used as the positive and blank control groups, respectively. The •OH scavenging efficiency was calculated according to the following equation:

$$\bullet \text{OH clearance rate}(\%) = \frac{A_0 - (A_S - A_C)}{A_0} \times 100\% \quad (5)$$

where A_0 and A_s are the absorbance of the blank control group and the samples at 510 nm, respectively. A_c is the absorbance of the control group treated with the ethanol solution of salicylic acid rather than $FeSO_4$.

DPPH• Clearance Test

The ethanol solution of DPPH (2 mL, 0.2 mM) was mixed with the samples (2 mL), then incubated at 37 °C for 30 min, away from light.[32] The absorbance of the solution at 517 nm was monitored. The control group was treated with ethanol (2 mL) rather than the ethanol solution of DPPH. AsA and DI water were used as the positive and blank groups, respectively. The DPPH• clearance rate was calculated as follows:

$$\text{DPPH} \bullet \text{ clearance rate } (\%) = \frac{A_0 - (A_s - A_c)}{A_0} \times 100\% \quad (6)$$

where A_s, A_c and A_0 denote the absorbance of the sample group, control group and blank group at 517 nm, respectively.

•$ABTS^+$ Clearance Test

The ABTS aqueous solution was diluted with an equimolar ratio of $K_2S_2O_8$ (2.45 mM) and allowed to stand away from light for 24 h.[33] Then, the mixture was further diluted to ensure that the absorbance at 734 nm was approximately 0.2. Next, the samples (20 μL, 2 mg mL^{-1}) were added to 96-well plates and incubated for 30 min. The absorbance at 734 nm was then determined. AsA and DI water were used as the positive and blank group, respectively. The •$ABTS^+$ scavenging ratio was calculated as follows:

$$\bullet \text{ABTS}^+ \text{clearance rate } (\%) = \frac{A_0 - A_S}{A_0} \times 100\% \quad (7)$$

where A_0 and A_s signify the absorbance of the blank control group and the sample group at 734 nm, respectively.

Synergistic Mucoadhesion Capacity

The amount of mucin absorbed was determined using the periodic acid Schiff (PAS) colorimetric method.[34] First, a calibration curve for mucin was created following the method described in the literature.[35] Next, mucin was dissolved in 0.20% (w/v) pH 2.0, 5.0 and 7.0 PBS under stirring for 6 h, respectively. Samples including free *trans*-Res, nanogels, and SA-Se/CL (Ngel made of SA-Se and crosslinked with CL as a counterpart. See Supporting Information for its preparation methods) were added to the mucin solution to achieve a concentration of 3 mg mL^{-1}. After incubation for 2 h with stirring, the solution was centrifuged at 12,000 rpm for 5 min to collect the supernatant. The UV–vis absorbance of the supernatant at 555 nm was measured, and the amount of unbounded mucin was calculated using the calibration curve. The difference between the initial added amount of mucin and the unbound mucin was considered as the mass of mucin absorbed.

In vitro Bioaccessibility of *Trans*-Res

In vitro Release Behavior

The release behavior of *trans*-Res was investigated using the mediums including (a) simulated intestinal fluid (SIF), (b) simulated gastric fluid (SGF)+SIF and (c) SGF+ simulated duodenal fluid (SDF)+SIF. For example, in case (c), the lyophilized Ngel-3@Res powder (6 mg) was dissolved in 2 mL SGF. The solution was then transferred into a dialysis bag (Molecular weight cut-off: 1000 Da), sealed its both ends and immersed in a beaker containing 10 mL SGF as the release medium. The release experiment was conducted at 37 °C. After 2 h, the pH of the system was adjusted to 5.0 using NaOH (1 M) and trypsin. 1 h later, the pH was continuously adjusted to 7.0 to simulate the pH in the colon. Throughout the process, 200 μL of the dialysate was extracted at predetermined time intervals and supplemented with an isometric new-made medium to maintain a constant total amount of release medium. The cumulative release amount of *trans*-Res was calculated as follows:

$$\text{Cumulative } trans-\text{Res release } (\%) = \frac{\text{released amount of } trans-\text{Res in medium at time t}}{\text{total amount of } trans-\text{Res in Ngel@Res}} \times 100\% \quad (8)$$

Toxicity Evaluation and Antioxidant Mechanism of Ngel and Ngel@Res

Culture of *C. elegans*

The culture and synchronization were performed according to the method proposed by Chen et al.[36]

Lifespan Test

The synchronized worms (L4) were randomly divided into 6 groups, with thirty worms in each group. They were then incubated with different concentrations of *trans*-Res or nanogel suspensions including Ngel-3, Ngel-3@Res with low (40 μg mL^{-1}), moderate (400 μg mL^{-1}) and high (1000 μg mL^{-1}) concentration (referred to as LC Ngel-3@Res, MC Ngel-3@Res and HC Ngel-3@Res). Throughout the tests, the nematodes were transferred to new-made medium, and the survival rate was calculated per 48 h using equation (9). Worms were considered dead if they did not respond to touch.

$$\text{Survival rate } (\%) = \frac{\text{the number of living } C.\ elegans}{\text{the total number of } C.\ elegans} \times 100\% \quad (9)$$

Movement Capacity

The nematodes were divided into 4 groups, each group consisting of twenty nematodes. These groups were exposed to *trans*-Res, Ngel-3, and HC Ngel-3@Res for a duration of 7 days. Then, the appropriate amount of M9 buffer was added. The nematodes that did not receive any treatment were served as the control group. The number of sinusoidal movements within 30 s was counted under a microscope to assess the impact of each sample on the motility of *C. elegans*. The experiments were performed thrice.

Acute Oxidative Stress Resistance

The influence of oxidative stress on *C. elegans* was investigated using the H_2O_2 method.[37] Initially, *C. elegans* were exposed to different samples, namely Ngel-3, and HC Ngel-3@Res for 7 days before conducting the experiments. Subsequently, the nematodes were transferred to a plate with a density of five nematodes in each well, and 1 mL PBS containing 40 mM H_2O_2 was added. The nematode death criterion was the same as that used in the lifespan experiment. The survival of the nematodes was assessed per 30 min using equation (9) as described in the "lifespan test" section under the aforementioned conditions. The experiments were performed thrice.

Determination of Antioxidases Activity and Malondialdehyde (MDA) Content

Catalase (CAT), superoxide dismutase (SOD) and glutathione peroxide (GSH-Px) were chosen as representative antioxidases. *C. elegans* (N2, wildtype, L4) were exposed on free *trans*-Res, Ngel-3, and HC Ngel-3@Res. After 7 days, the nematodes were washed with M9 buffer. The homogenate was ultrasonically crushed and centrifuged to collect the supernatant for detecting the activity of antioxidases using their specific detection kits (Nanjing Jiancheng, China). The MDA content was measured using a specific kit (Nanjing Jiancheng, China), following the provided instructions. Three parallel tests were conducted for each group.

Fluorescence Observation of *C. elegans*

The nematodes (L4) were divided into 4 groups: control group, *trans*-Res group, Ngel-3 group, and HC Ngel-3@Res group and exposed for 7 days, the nematodes were then washed with M9 buffer thrice. Afterwards, they were transferred into a 24-well plate and incubated with the fluorescence probe (DCFH-DA, 1 mL, 50 μM) at 20°C for 1 h, away from light. The nematodes were then rinsed thrice using M9 buffer to remove the residual DCFH-DA. The well-washed nematodes were picked onto slides and anesthetized with a new-made levamisole solution (l μL, 60 μM) and covered with a coverslip. The nematodes were observed on a laser confocal fluorescence microscope, and fluorescence images were captured at an excitation wavelength of 485 nm. Ten nematodes were randomly selected from each group for picture-taking, and the relative fluorescence intensity was quantitatively analyzed by ImageJ software.

qRT-PCR Test

Prior to determination, *C. elegans* (L4) were incubated with the samples, including *trans*-Res, Ngel-3 and HC Ngel-3@Res for 7 days. Afterwards, RNA of *C. elegans* was isolated using Trizol. The qRT-PCR experiment was then conducted on a MyGo Pro Real-Time PCR Detection System (ABI, England). The fold changes of gene expression were detected using the comparative CT method and an iTaq Universal SYBR Green one-step kit. All experiments were repeated thrice. The primers used in this study were listed in Table S1.

Statistical Analysis

The resulting results were presented as the form of "average value ± standard derivation". Statistical differences in lifespan, motility, endogenous ROS content, antioxidase activity, MDA content and mRNA level were indicated by p-values (*, ** and *** denoting $p<0.05$, $p<0.01$ and $p<0.001$, respectively), calculated and plotted by GraphPad Prism 8.0.2 software. The *** signified a significant difference in the results.

Results

Preparation and Characterization of Nanogels

The nanogels were prepared using selenized thiolated SA (TSA-Se) through crosslinking with CL for the intestinal targeted delivery of *trans*-Res (Figure 1A). The chemical structure of Ngel and its precursors was confirmed by ^{1}H NMR and FTIR spectra, respectively. In the ^{1}H NMR spectrum of SA (Figure S1), only chemical shifts of the methyne proton and methyl protons positioned at 3.6 ppm and 1.1 ppm, respectively, were observed. However, in the TSA spectrum, shifts attributed to the methylene of MTA were found at 3.3 ppm, suggesting the successful conjugation of MTA on the skeleton of SA to obtain TSA. The content of -SH group was 592.6±3.3 μmol·(gm)$^{-1}$ from Ellman's test. Additionally, in the FTIR spectrum of SA (Figure 1B), the peaks appeared at 3000~3700, 1650~1740 and 1400 cm^{-1} belonging to stretching vibration of -OH in carboxy, -C=O and the asymmetric stretching vibration of -COOH, as well as the symmetric stretching vibration of -COOH were visible. A new peak at 2668 cm^{-1}, caused by -SH after sulfhydrylation, further indicated the formation of TSA. The characteristic peaks of TSA-Se resembled those of TSA, with the exception that the featured peaks of -OH stretching vibration occurred at a red-shift from 3376 cm^{-1} (TSA) to 3358 cm^{-1} (TSA-Se). The bending vibration of -OH also shifted towards the low frequency (from 1622 cm^{-1} to 1598 cm^{-1}), indicating the interaction between TSA and Se derived from the reduction of Na_2SeO_3 by AsA.[38] Therefore, the formation mechanism of TSA-Se was elucidated as follows: firstly, the -OH of carboxyl groups in the TSA skeleton reacted with -SeO_3^{2-} to form chain intermediates, followed by the formation of Se via AsA reduction and subsequent aggregation to form the inner core of Se NPs. Finally, TSA-Se was formed with TSA surrounding the Se core.[28] The absorption bands at 2875~2985 cm^{-1} were observed due to C-H stretching vibration, confirming the formation of TSA-Se. As for *trans*-Res, the peaks at 830, 960 and 1154 cm^{-1} indicated the presence of -C=CH, -C-O and -C-C- of benzene skeleton, respectively. Moreover, the peak of phenolic -OH was visible at 3300–3500 cm^{-1}. After crosslinking, the intensity of both symmetric (2895 cm^{-1}) and asymmetric (2983 cm^{-1}) stretching vibrations of TSA-Se decreased, and all the peaks in the absorption bands ranging from 1720 to 1130 cm^{-1} shifted towards lower wavenumbers. The decrease in intensity was due to the spatial effect, demonstrating that the formation of a calcium alginate crosslinking layer. These Results demonstrate the successful synthesis of the nanogels. The FTIR spectrum of Ngel@Res exhibited the characteristic peaks of both TSA-Se

and *trans*-Res to confirm *trans*-Res encapsulation. In Figure 1C and Table S2, the D_h was 188.75 ± 7.57, 162.35 ± 5.83 and 120.36 ± 4.37 nm for Ngel-1, Ngel-2 and Ngel-3, respectively. After *trans*-Res loading, these values increased to 283.60 ± 2.58, 232.18 ± 1.79 and 260.32 ± 0.56 nm in the same order, preliminarily indicating the introduction of hydrophobic *trans*-Res. The PDI was 0.217 ± 0.037 for Ngel-1, 0.202 ± 0.056 for Ngel-2, 0.183 ± 0.042 for Ngel-3, and 0.386 ± 0.041 for Ngel-1@Res, 0.305 ± 0.028 for Ngel-2@Res, 0.189 ± 0.029 for Ngel-3@Res after *trans*-Res encapsulation, respectively. The D_h curve of the suspensions showed a narrow single-peak, indicating an uniform particle size distribution. In Figure 1D, both TSA and TSA-Se had a negatively charged ζ-potential with absolute values of 9.9 ±0.5 and 8.8±0.9 mV, respectively, owing to the presence of carboxyl groups, further suggested that the negatively charged TSA was immobilized on the surface of Se NPs.[28] *Trans*-Res had a ζ-potential of 2.1±1.6 mV. After crosslinking, the negative charges of -COOH were neutralized by Ca^{2+}, resulting in a reduction to −6.1±0.5 mV for Ngel-3. Ngel-3@Res showed a 6.0±0.2 mV of ζ-potential as the introduction of *trans*-Res. These negatively charged Ngel-3 and Ngel-3@Res are liable to electrostatic interaction with the positively charged inflammatory mucus.[39] As shown in Figure 1E, the XRD patterns of *trans*-Res were visible at 2Θ=6.56°, 13.06°, 16.08°, 18.96°, 22.15°, 23.28° and 28.07°.[16,40] Upon the formation of Ngel-3@Res, these diffraction peaks of *trans*-Res disappeared, and some new peaks, including two amorphous dispersion peaks at 2Θ=8.32°, 22.04° and a new crystal peak at 2Θ=42.57° emerged. These changes indicate that the interactions between TSA-Se and CL altered the crystallization of *trans*-Res by disrupting the solid molecular arrangement of the TSA-Se chain. Furthermore, the morphology and the content, distribution of the featured elements including C, O, Ca, S, Se in nanogels were observed by TEM and EDS, respectively. The Ngel-3 exhibits spherical morphology with an average diameter of 110.12 ± 5.42 nm (Figure 2A). The Ngel-3@Res also possessed the same morphology but some spots attributed to hydrophobic *trans*-Res caused an increase in D_h to 230.45±3.12 nm after *trans*-Res loading (Figure 2B). When the Ngel-3@Res was digested using SGF for the first 2 h, it still maintained its shape (Figure 2C). The contours of the Ngel-3@Res became blurred and piled up after treatment with SIF for 2 h (Figure 2D), followed by the formation of a platelike texture and the release of *trans*-Res after incubation with SIF for another 2 h (Figure 2E and F). These results confirm that Ngel-3@Res showed promise in protecting *trans*-Res from the harsh gastric environment and achieving intestinal targeted *trans*-Res release. We also captured EDS elemental maps of Ngel-3@Res exposed to the electron beam, which provide solid evidence that the presence of C, O, Ca, S and Se elements (Figure 2G–K), their overlay image is shown in Figure 2L. The morphology of Ngel-3@Res in Figure 2G–L is slightly different from that in Figure 2B, which is caused by the bombardment of the high-temperature ion beam. The degree of morphology change is exponentially correlated with the temperature of the beam.[41] The relative content of S and Se elements in Ngel-3@Res analyzed by EDS mapping was 98.63% and 1.37%, respectively.

Trans-Res Loading Behavior

Due to the hydrophobicity of *trans*-Res, the unloaded *trans*-Res was separated by centrifugation. The LC of Ngel-1@Res, Ngel-2@Res and Ngel-3@Res using in situ loading method was measured to be 43.56 ± 1.44%, 47.82 ± 0.79% and 50.33 ± 0.56%, respectively. The EE values for *trans*-Res loaded nanogels were 89.25 ± 1.36%, 87.41 ± 2.24% and 90.56 ± 3.53% in the same order as above, indicating that the well-synthesized nanogels are highly suitable for *trans*-Res encapsulation.

Stability Assay

pH Stability

Trans-Res is stable under acidic conditions, while degrades under alkaline environments.[42] The retention rate of *trans*-Res was 70.11 ± 3.31% at pH 2.0, 72.62 ± 3.81% at pH 5.0 and 32.25 ± 4.11% at pH 7.0, respectively, pronouncedly lower than that of *trans*-Res with the protection of Ngel-3, which reached up to 95.63 ± 4.18%, 87.64 ± 3.74% and 43.57 ± 4.19% for pH 2.0, 5.0 and 7.0 (Figure 3A–C and their insets). These results demonstrate that loading *trans*-Res in Ngel effectively improved its pH stability in acidic environment, which were also confirmed by the morphological changes of Ngel-3@Res in simulated gastrointestinal fluids (Figure 2C–F).

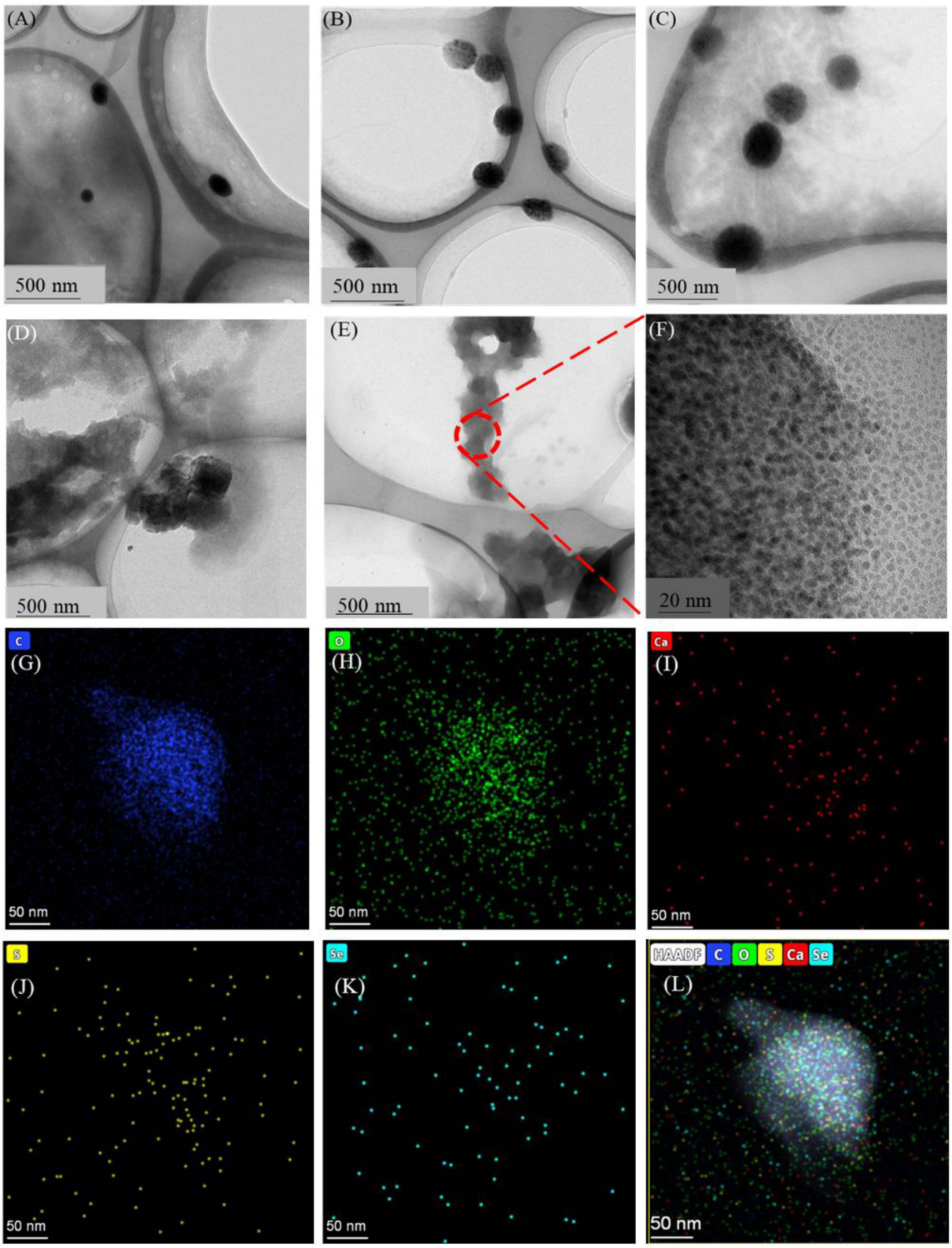

Figure 2 TEM photographs of (**A**) Ngel-3, (**B**) Ngel-3@Res. Ngel-3@Res digested by SGF for (**C**) 2 h, followed by treatment with SIF for (**D**) 2 h and (**E**) 4 h, respectively. (**F**) Partial enlarged view of Figure (**E**). EDS elemental maps of C, O, Ca, S, Se element of Ngel-3@Res (**G**–**K**) and their overlay image (**L**).

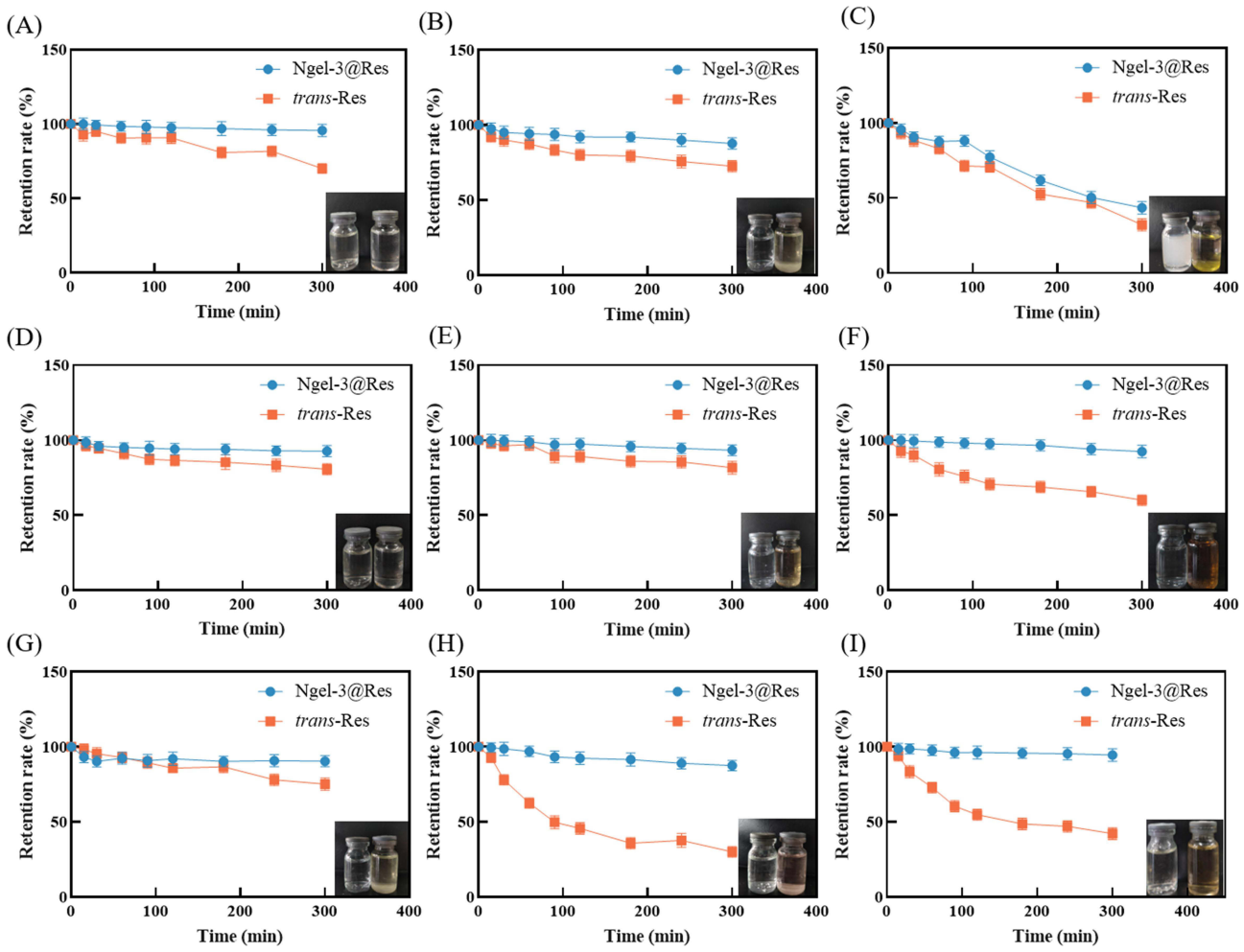

Figure 3 The influence of pH, temperature, ultraviolet radiation and redox agents on the retention rate of *trans*-Res with or without Ngel-3 protection during 5 h incubation. pH: (**A**) 2.0, (**B**) 5.0 and (**C**) 7.0; Temperature: (**D**) 25 °C, (**E**) 37 °C and (**F**) 60°C; Redox: (**G**) 1.0% H_2O_2, (**H**) 0.20% Na_2SO_3 and (**I**) ultraviolet radiation. The inset at the lower right corner of each picture presents the appearance of Ngel-3@Res (left) and *trans*-Res (right) after corresponding treatment.

Temperature Stability

When the temperature is lower than 60 °C, there is no obvious color change and precipitation of *trans*-Res with the protection of Ngel-3 (Figure 3D and E and their insets). When free *trans*-Res was treated in water bath at 25, 37 and 60°C, the residue amount was only 80.73 ± 3.81%, 81.70 ± 4.25% and 60.11 ± 3.51%, respectively (Figure 3D–F). This decrease can be ascribed to the high temperature, which accelerates the failure of *trans*-Res. By contrast, when *trans*-Res was protected by Ngel, the residue amount still maintained 92.64 ± 3.74%, 93.32 ± 3.63% and 92.49 ± 4.19% in the same order. Compared to free *trans*-Res, the retention rate of *trans*-Res with Ngel-3 protection increased by 11.91%, 11.62% and 34.38%, respectively. Notably, the protective effect of Ngel-3 on *trans*-Res became more pronounced at 60 °C. This finding is consistent with Shankar's results, which found that calcium alginate is highly conducive to enhance the activity of *Aspergillus terreus*$_{GR}$ α-galactosidase at 60 °C.[43]

Redox Stability

The retention amount of *trans*-Res was 75.25±4.11% after incubation with 1.0% H_2O_2, and that was 30.11±3.51% when trans-Res was exposed on 0.20% Na_2SO_3. It is noteworthy that Ngel-3 significantly increased the retention of *trans*-Res to 90.45 ± 3.59% and 87.59±3.45% under oxidizing and reducing conditions, respectively (Figure 3G and H). These results were similar to the those observed with *Polygonatum sibiricum* polysaccharide stabilized Se NPs, which possessed a higher protective effect against H_2O_2-induced PC-12 cell death,[28] indicating that seleno-polysaccharide could scavenge H_2O_2 effectively.

Compared with free *trans*-Res, the aqueous solution of *trans*-Res with Ngel-3 protection did not show obvious color change and precipitation after redox treatment (Figure 3G and H and their insets).

Ultraviolet Stability

UV irradiation can induce various chemical reactions such as isomerization, cycloaddition, photorearrangement, hydroxylation and *cis*-cyclization.[44] As a result, the retention rate of *trans*-Res after 5 h of UV radiation is only 42.45 ± 4.11%, which is unsatisfactory for its application (Figure 3I and its inset). When *trans*-Res was protected by Ngel-3, the content of *trans*-Res reached up to 94.57 ± 4.18% under the same treatment.

Synergistic Free Radical Scavenging Effects

Firstly, the antioxidant effects of the component of Ngel were determined. As shown in Figure 4A, the clearance rate of SA to •OH and •DPPH was 69.32±0.13%, 41.86±0.33%, and that of TSA was 71.12±0.30% for •OH, 61.42±0.14% for •DPPH, respectively, showed almost no scavenging effects on $•ABTS^+$. Note that TSA-Se-3 had a satisfying scavenging ratio of up to 97.09±1.68% for •OH, 53.57±0.46% for •DPPH and 87.58±0.49% for $•ABTS^+$, the increase in free radical scavenging capacity of TSA-Se compared with TSA was due to selenization.[45] Afterwards, the effect of Se content in Ngel on its free radical scavenging efficacy was investigated, and a suitable Ngel was required to be screened by free radical clearance efficacy for follow-up experiments. Regarding its free radical scavenging performance, they exhibited Se concentration-dependent clearance features, so Ngel-3 with the highest Se content among various Ngel samples had the best radical scavenging ratio (Figure 4B). However, the significantly decreased free radical clearance capacity of Ngel-3 compared with that of TSA-Se-3 is attributable to the calcium alginate layer enclosing most of TSA-Se and hindering the implementation of its antioxidant effects. Furthermore, *trans*-Res showed almost 100% clearance rate against •DPPH and $•ABTS^+$ radicals but no clear effect on •OH without mimic digestion. It is very gratifying to see that the general free radical scavenging effect against •OH (60.27±0.19%), •DPPH (33.67±0.53%), and $•ABTS^+$ (43.70 ±0.32%) occurred with the protection of Ngel-3 (Figure 4C). After digestion, *trans*-Res possessed 2.88±1.00% for •OH clearance rate, 33.42±2.95% for •DPPH and 40.64±0.14% for $•ABTS^+$, respectively. As for Ngel-3@Res, the calcium alginate layer was destroyed, leading to a complete exposure of TSA-Se and *trans*-Res, thereby resulting in a broad-spectrum clearance efficacy for •OH (99.11±0.61%), •DPPH (55.11±0.56%) and $•ABTS^+$ (59.88±0.80%), respectively (Figure 4D). The synergistic free radical clearance performance of Ngel-3@Res confirms that the antioxidant effect of *trans*-Res was well supplemented by antioxidative Ngel.

Mucoadhesion Behavior

The amount of mucin absorbed by *trans*-Res, Ngel-3, and Ngel-3@Res was determined at pH 2.0, 5.0 and 7.0, respectively, as shown in Figure 4E. Compared to the negligible amount of mucin absorbed by *trans*-Res and SA-Se /CL, which was 46.30 ± 0.79 μg for Ngel-3 and 54.87 ± 0.37 μg for Ngel-3@Res at pH 2.0, respectively. Subsequently, the amount of mucin absorbed by Ngel-3 and Ngel-3@Res increased to 66.89 ± 0.20 μg and 89.39 ± 0.79 μg at pH 5.0, respectively, while the value of *trans*-Res and SA-Se/CL remained unchanged. At pH 7.0 (>pKa of 2.6), 49.15 ± 0.65 μg of mucin was absorbed by *trans*-Res.[46] The adhesion amount of SA-Se/CL was only 9.75 ± 0.15 μg. The absorption of Ngel-3 slightly increased to 72.85 ± 0.46 μg. It is worth noting that the mucin adsorption of Ngel-3@Res increased significantly to 140.70 ± 0.53 μg.

In vitro *Trans*-Res Release

The release profiles of *trans*-Res from Ngel-3@Res in various of mediums are shown in Figure 4F–H. When Ngel-3@Res was exposed to SIF, an initial explosive release of *trans*-Res within 1 h, followed by a plateau, the cumulative *trans*-Res release amount reached 87.40 ± 2.89% by the end of the entire release process (Figure 4F), suggesting that the calcium alginate layer was degraded by SIF and provided diffusion paths for *trans*-Res to disperse outward. When Ngel-3@Res was initially immersed in SGF, the crosslinked layer was well preserved for 2 h, which is in agreement with the TEM results (Figure 2C). The release amount was only 9.88 ± 2.00%, signifying the effective protection of Ngel on *trans*-Res in harsh stomach conditions. Subsequently, a rapid release occurred in SIF stage, resulting in 83.75 ± 3.41%

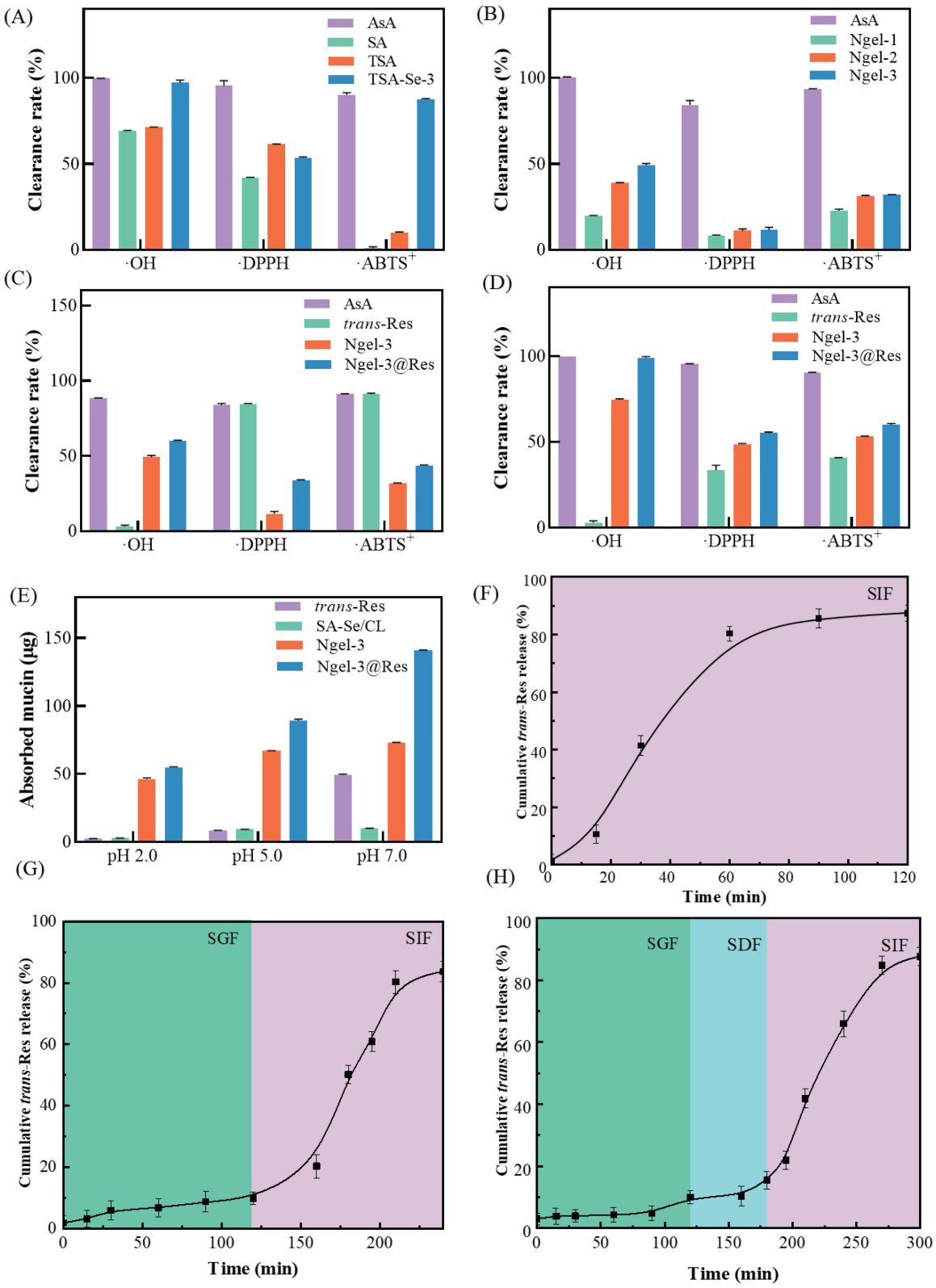

Figure 4 (**A**) SA, TSA, TSA-Se-3 and (**B**) Ngel with different Se concentrations against representative free radicals including •OH, •DPPH, and •ABTS$^+$. The representative free radical scavenging rate of the samples, including *trans*-Res, Ngel-3 and Ngel-3@Res before (**C**) and after (**D**) simulated gastrointestinal digestion. AsA was used as control group. The amount of mucin absorbed by *trans*-Res, SA-SeKGM/CL nanogel, Ngel-3 and Ngel-3@Res at pH 2.0, 5.0 and 7.0 (**E**). The release curves of *trans*-Res from Ngel-3@Res in the medium that simulates intestinal (**F**), gastric and intestinal (**G**), and gastric, duodenal and intestinal (**H**) microenvironments.

trans-Res being released (Figure 4G). We also investigated the release behavior of Ngel-3@Res in the medium composed of SGF, SDF and SIF. Similar to the profile shown in Figure 4G, the total release amount of *trans*-Res was less than 15.44%, further demonstrating that the protective effect of Ngel on *trans*-Res in both the SGF and SDF stages, following a readily release of *trans*-Res occurred in SIF, reached to 87.67 ± 2.90% of *trans*-Res being released from Ngel-3@Res at 5 h (Figure 4H), indicating that Ngel could enable intestinal targeting with *trans*-Res.

Toxicity and Antioxidant Mechanism of Ngel and Ngel@Res

Lifespan of *C. elegans*

The mean, median and maximum lifespan of *C. elegans* were measured when exposed to *trans*-Res, Ngel-3 and Ngel-3@Res with different concentrations, as shown in Figure 5A and Table 1. Compared with the control, *trans*-Res and Ngel-3 groups, Ngel-3@Res nanogels with different concentrations could prolong the mean, median and maximum lifespan of *C. elegans* (Table 1). Specifically, the maximum lifespan of *C. elegans* incubated with *trans*-Res and Ngel-3 was 24.00 ± 1.17 and 26.00 ± 2.17 days, respectively, which were still lower than that of those treated with Ngel-3@Res (26.00 ± 3.52 days for LC, 26.00 ± 3.57 days for MC and 26.00 ± 4.27 days for HC samples) (Table 1). These results suggest a remarkable extension of the lifespan of *C. elegans* when incubated with Ngel-3@Res nanogels, particularly with HC Ngel-3@Res; therefore, HC Ngel-3@Res was screened for the follow-up experiments.

Acute Oxidative Stress

Under the induction of the excessive H_2O_2, the mean survival time of untreated *C. elegans* was only 2.00 ± 0.36 h. However, the mean survival times of *C. elegans* exposed to *trans*-Res, Ngel-3 and HC Ngel-3@Res reached up to 2.35 ± 0.33 h, 3.10 ± 0.28 h and 3.20 ± 0.32 h (Figure 5B), respectively, suggests that all samples showed a general H_2O_2 scavenging effect. Especially for HC Ngel-3@Res, which displayed the most profound increase in survival rate, owing to its synergistic H_2O_2 scavenging effect.

Movement Capacity

The movement frequency of *C. elegans* without treatment or treated with *trans*-Res, Ngel-3 and HC Ngel-3@Res in 30s was 32.67±1.53, 30.33±1.53, 33.00±2.00 and 32.00±2.00, respectively (Figure S2). There was almost no difference in movement behavior between any two groups, indicating that Ngel-3 and HC Ngel-3@Res did not affect the movement ability and indirectly confirming their biosafety.

ROS Clearance Capacity in *C. elegans*

Firstly, the total ROS content in *C. elegans* was measured qualitatively using fluorescence imaging. Since the fluorescence intensity is proportional to ROS concentration in *C. elegans*, it was observed that the fluorescence intensity followed the order of HC Ngel-3@Res<Ngel-3<*trans*-Res<control group (Figure 5C–F); therefore, the ROS amount in *C. elegans* was found to be in the same sequence (Figure 5G). These results are consistent with the antioxidant performance of *trans*-Res, Ngel-3 and Ngel-3@Res as described above (Figure 4B–D). Subsequently, the activity of antioxidases including SOD, CAT and GSH-Px was determined quantitatively after incubation with *trans*-Res, Ngel-3 and HC Ngel-3@Res. Specifically, SOD decomposes $\bullet O^{2-}$ into H_2O_2 and O_2, following the disintegration of H_2O_2 into H_2O and O_2 by CAT.[47,48] GSH-Px catalyzes the transformation of GSH to GSSG, converting the toxic peroxides into non-toxic hydroxyl compounds. This process promotes the decomposition of H_2O_2, protecting the structure and function of the cell membrane from interference and damage caused by peroxides.[49] The activity of SOD, CAT and GSH-Px in *C. elegans* treated with *trans*-Res, Ngel-3 and HC Ngel-3@Res showed a continuous increase (Figure 5H–J). Specifically, the results indicated an increase in SOD activity by 23.74% for *trans*-Res, 34.87% for Ngel-3 and 40.32% for HC Ngel-3@Res treated group compared to the control group (Table 2). Similarly, the activity of CAT also showed a considerable improvement of 78.94%, 191.05% and 196.32% for the respective sample groups in the same sequence as mentioned above (Table 2), compared to the control group. The activity of GSH-Px showed the same trend (Table 2). Conversely, the MDA content in *C. elegans* was inversely proportional to the activity of antioxidases

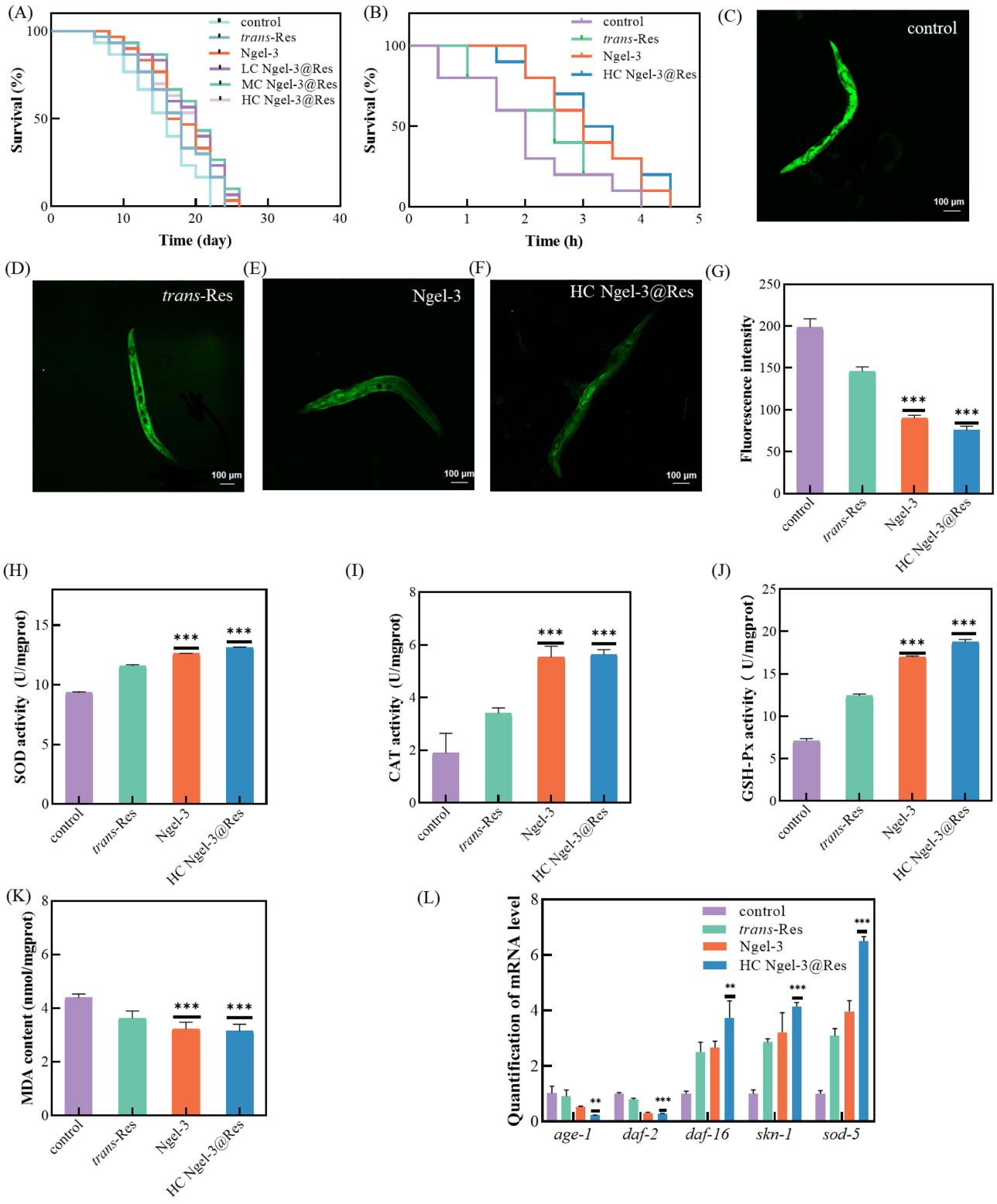

Figure 5 (**A**) The lifespan of *C. elegans* exposed to *trans*-Res, Ngel-3 and Ngel@Res at different concentrations. (**B**) The survival time of *trans*-Res, Ngel-3 and HC Ngel-3@Res treated *C. elegans* under oxidative stress. (**C–F**) Fluorescence images and (**G**) fluorescence intensity of *C. elegans* in (**D**) control group, and *C. elegans* treated with (**D**) *trans*-Res, (**E**) Ngel-3 and (**F**) HC Ngel-3@Res after 7 days. The activity of antioxidases such as (**H**) SOD, (**I**) CAT and (**J**) GSH-Px, as well as (**K**) the content of MDA in *C. elegans* incubated with *trans*-Res, Ngel-3 and HC Ngel-3@Res after 7 days. (**L**) Effect of *trans*-Res, Ngel-3 and HC Ngel-3@Res on gene expression levels of *daf-2, age-1, daf-16, sod-5* and *skn-1* in N2 nematodes by qRT-PCR. Untreated *C. elegans* were used as control group. *, ** and *** represent $p<0.05$, $p<0.01$ and $p<0.001$, respectively.

https://doi.org/10.2147/IJN.S464849 DovePress

Table 1 The Lifespan of *C. elegans* Exposed on *trans*-Res, Ngel and Various of Ngel-3@Res Nanogels by Kaplan-Meier Survival Analysis Using SPSS Software

Lifespan (Days)	Control	*trans*-Res	Ngel-3	LC Ngel-3@Res	MC Ngel-3@Res	HC Ngel-3@Res
Mean lifespan	17.07±0.94	15.13±0.90	17.93±0.88	18.80±0.92	19.40±0.88	18.53±0.98
Median lifespan	18.00±1.00	18.00±1.34	16.00±1.12	20.00±1.07	20.00±1.09	20.00±1.81
Maximum lifespan	22.00±1.88	24.00±1.17	26.00±2.17	26.00±3.52	26.00±3.57	26.00±4.27
P value vs control	n. a.	n.s.(0.067)	*	*	**	*

Notes: *p<0.05; **p<0.01.
Abbreviations: n. a., not applicable; n. s., not significant.

Table 2 Results of Antioxidases Activity of Nematodes

Sample	SOD			CAT			GSH-P_X		
	Activity (U/mgprot)	Rate of Change (%)	P value	Activity (U/mgprot)	Rate of Change (%)	P value	Activity (U/mgprot)	Rate of Change (%)	P value
Control	9.35±0.07	–	–	1.90±0.74	–	–	7.09±0.26	–	–
***trans*-Res**	11.57±0.13	**Increase** 23.74	***	3.40±0.21	**Increase** 78.94	***	12.39±0.24	**Increase** 74.75	***
Ngel-3	12.61±0.03	**Increase** 34.87	***	5.53±0.42	**Increase** 191.05	***	17.00±0.12	**Increase** 139.77	***
HC Ngel-3@Res	13.12±0.06	**Increase** 40.32	***	5.63±0.19	**Increase** 196.32	***	18.74±0.32	**Increase** 164.32	***

Note: ***p<0.001.

(Figure 5K), demonstrating the remarkable ROS scavenging effect of Ngel-3 and HC Ngel-3@Res. This also confirms the improvement of Ngel-3 on the bioactivity of *trans*-Res.

qRT-PCR Experiments

qRT-PCR was performed to investigate the effects of Ngel-3 and HC Ngel-3@Res on the expression levels of *daf-2*, *age-1*, *daf-16*, *skn-1* and *sod-5* mRNA. Figure 5L shows Ngel-3 and HC Ngel-3@Res decreased the expression levels of aging genes including *daf-2* and *age-1*, sharply improved the expression levels of anti-aging gene *daf-16* and the representative superoxide dismutase genes such as *sod-5* and *skn-1*,[50] compared with the control group.

Discussion

In acidic environment, the carboxyl groups in Ngel become protonated, leading to increased hydrogen bonding interactions and the resultant Ngel contraction, providing protection against acid degradation for *trans*-Res. As the pH increases, electrostatic repulsion occurs between the gradually deprotonated carboxyl groups, leading to increased hydrogen bonding interactions and further contraction of Ngel, offering better protection for *trans*-Res in acidic microenvironment. Meanwhile, the enhanced electrostatic repulsion occurred between the completely deprotonated carboxyl groups causes the breakdown of the calcium alginate layer, creating paths for the outward diffusion of *trans*-Res, resulting in a decrease in retention rate. *Trans*-Res is stable at room temperature and body temperature, however, the hydroxyl and double bonds in its structure readily undergo reaction at high temperatures, resulting in decomposition. Consequently, the solution of *trans*-Res acquires a brown color.[51] When *trans*-Res is exposed to high temperatures, Ngel act as a barrier between *trans*-Res and the external environment, preventing high-temperature induced decomposition. Both TSA-Se and its crosslinked layer with CL provide a reliable shielding effect, enhancing *trans*-Res's redox resistance during processing and storage. The inherent antioxidant property of Ngel allows the antioxidant capacity of *trans*-Res to be retained. *Trans*-Res, commonly used as a functional food additive, is susceptible to degradation by UV radiation. The protection provided by Ngel results in close to 100% retention of *trans*-Res after UV exposure, attributed to the scattering of UV light by hydroxyls and ester bonds in Ngel, which enhances the UV resistance stability of *trans*-Res by reducing the UV radiation intensity to *trans*-Res.

Trans-Res demonstrates a notable scavenging effect on •OH and •DPPH, although this effect is significantly diminished after simulated gastroenteric digestion. It is important to highlight that Ngel-3 exhibits a broad-spectrum scavenging capacity for •OH, •DPPH, and •$ABTS^+$, which is further enhanced after digestion, confirming the inherent ROS scavenging potential of Ngel. Ngel can compensate for the absence of antioxidant effects of *trans*-Res. The antioxidant capacity of Ngel-3@Res is notably elevated before and after digestion compared to Ngel-3 or *trans*-Res, suggesting that the protection of Ngel can augment the antioxidant activity of *trans*-Res.

The nanogels we prepared were designed for intestinal targeted delivery of *trans*-Res through intestinal mucoadhesion. Regardless of the pH, only a limited amount of mucin was absorbed by *trans*-Res. At pH 2, it can be inferred that the adhesion mechanism of Ngel-3 and Ngel-3@Res primarily relies on covalent adhesion through the formation of disulfide bonds between thiol in TSA-Se and thiol in mucin, rather than non-covalent adhesion through hydrogen bonding and Van der Waals' interactions. At pH 5, the mucin adhesion of Ngel-3 and Ngel-3@Res increased further, confirming that the mucoadhesion of Ngel-3 was mainly through covalent adhesion. At pH 7.0, SA-Se, TSA-Se and *trans*-Res were exposed upon the destruction of the calcium alginate layer of SA-Se/CL, Ngel-3 and Ngel-3@Res. Then, the -SO^{3-} and -COO^- groups in mucin adhered to the positively charged *trans*-Res through electrostatic effect. Due to the absence of -SH groups and the ionization-induced electrostatic repulsion between SA-Se and mucin, the adsorption amount of mucin by SA-Se/CL can be ignored. The adsorption amount of 140.70 ± 0.53 μg mucin is caused by both electrostatic adhesion between mucin and *trans*-Res, as well as covalent adhesion between TSA-Se and mucin. The calcium alginate cross-linked layer of Ngel@Res is gradually destroyed with the digestion of simulated gastric, duodenum, and colon fluids, providing release paths for the intestinal targeted release of *trans*-Res.

Compared with *trans*-Res, Ngel-3 and Ngel-3@Res not only significantly extend the mean, median and maximum lifespan of *C. elegans*, but also demonstrate no negative effects on movement, indicating the biosafety of the nanogels. Additionally, the nanogels enhance the activity of antioxidases in *C. elegans* and reduce the content of MDA, a product of lipid peroxidation, suggesting the synergistic antioxidant capacity of Ngel and *trans*-Res. The insulin/IGF-1 signaling (IIS) pathway, known as the most typical pathway regulating lifespan in most species,[52] is influenced by Ngel and Ngel@Res through down-regulation of the aging genes *daf-2* and *age-1*, moreover, they significantly up-regulate the anti-aging gene *daf-16* and the representative superoxide dismutase genes (*sod-5* and *skn-1*).[50] The effective anti-aging effect of the nanogels was confirmed through antioxidation perspective.

A previous study showed that *trans*-Res loaded starch-based Pickering emulsions resulted in a decrease in •DPPH scavenging activity, possibly due to high temperatures during preparation.[3] Fortunately, our preparation does not require high temperatures; moreover, *trans*-Res was endowed with the enhanced broad-spectrum antioxidant properties both before and after digestion by the selenized thiolated alginate-based nanogels, the free radical scavenging activity was significantly enhanced. Wang et al developed lecithin-polysaccharide self-assembled microspheres for *trans*-Res loading. While the free radical scavenging activity of this system was improved prior to gastrointestinal digestion, its antioxidant capacity post-digestion remains unknown,[8] and there was a lack of relevant in vivo activity evaluation. The biosafety of Ngel and Ngel@Res was assessed using *C. elegans* as model animals, and the potential applications in the anti-aging field were discussed based on antioxidant properties.

Conclusion

In this study, a selenized alginate-based intestinal targeted nanocarrier (Ngel) with broad spectrum ROS autonomous scavenging performance was constructed to improve the bioactivity of *trans*-Res. Ngel endowed pH, temperature, redox and ultraviolet irradiation resistance to *trans*-Res. Ngel@Res not only exhibited synergistic free radical scavenging efficacy against •OH, •$ABTS^+$, •DPPH after digestion using simulated gastrointestinal fluids, but also possessed the feature of the "stomach fold" and "intestine break", thereby facilitating intestinal targeted release of *trans*-Res and prolonging the retention time in the intestine through synergistic mucoadhesion. Due to the broad-spectrum autonomous ROS scavenging efficacy of Ngel and the synergistic antioxidant performance of Ngel@Res, treatment with Ngel-3 and HC Ngel-3@Res extended the lifespan of *C. elegans* to 26.00 ±2.17 and 26.00±4.27 days, respectively, and accompanied by a significant increase in the activity of CAT, SOD and GSH-Px. qRT-PCR results indicated that both Ngel and Ngel@Res upregulated the expression of *daf-16*, *sod-5* and *skn-1*, while

downregulating the expression of *daf-2* and *age-1*. This study presents a promising paradigm to enhance the bioactivity of *trans*-Res and for further nutraceutical development.

Acknowledgments

The present work was supported by Engineering Research Center of Major Infectious Disease Therapeutics, Universities of Shaanxi Province. This work was also supported by the National Natural Science Foundation of China (No. 22308207), the Young Talent Fund of Xi'an Association for Science and Technology (No. 959202413044), the Natural Science Fundamental Research Program of Shaanxi Province (No. 2021JQ-550) and the Natural Science Research Fund of Shaanxi University of Science & Technology (No. 2019BJ-43). We also thank Prof. Liangbin Hu at School of Food Science and Engineering of Shaanxi University of Science & Technology for assisting with toxicity evaluation experiments.

Disclosure

The authors claim that there are no conflicts to declare.

References

1. Barreca D, Trombetta D, Smeriglio A, et al. Food flavonols: nutraceuticals with complex health benefits and functionalities. *Trends Food Sci Tech*. 2021;117:194–204. doi:10.1016/j.freeradbiomed.2021.03.027
2. Singh AP, Singh R, Verma SS, et al. Health benefits of resveratrol: evidence from clinical studies. *Med Res Rev*. 2019;39:1851–1891. doi:10.1002/med.21565
3. Wu B, Gu LY, Wang WJ, et al. Skin targeting of resveratrol-loaded starch-based Pickering emulsions: preparation, characterization, and evaluation. *Colloid Polym Sci*. 2021;299:1383–1395. doi:10.1007/s00396-021-04856-z
4. Wu B, Li Y, Li Y, et al. Pickering emulsions-chitosan hydrogel beads carrier system for loading of resveratrol: formulation approach and characterization studies. *React Funct Polym*. 2021;169:105674. doi:10.1016/j.reactfunctpolym.2021.105074
5. Sharkawy A, Casimiro FM, Barreiro MF, et al. Enhancing trans-resveratrol topical delivery and photostability through entrapment in chitosan/gum Arabic Pickering emulsions. *Int J Biol Macromol*. 2020;147:150–159. doi:10.1016/j.ijbiomac.2020.01.057
6. Gowd V, Kanika, Jori C, et al. Resveratrol and resveratrol nano-delivery systems in the treatment of inflammatory bowel disease. *J Nutr Biochem*. 2022;109:101. doi:10.1016/j.jnutbio.2022.109101
7. Wang -P-P, Luo Z-G, Tamer TM. Spiral-dextrin complex crystals: efficient approach for colon-targeted resveratrol delivery. *J Agric Food Chem*. 2020;69:474–482. doi:10.1021/acs.jafc.0c05668
8. Wang L, Lai C, Li D, et al. Lecithin-polysaccharide self-assembled microspheres for resveratrol delivery. *Antioxidants*. 2022;11:69–88. doi:10.3390/antiox11091666
9. Chedea VS, Vicas SI, Sticozzi C, et al. Resveratrol: from diet to topical usage. *Food Funct*. 2017;8:3879–3892. doi:10.1039/c7fo01086a
10. Qi X, Yang N, Luo Y, et al. Resveratrol as a plant type antioxidant modifier for polysulfone membranes to improve hemodialysis-induced oxidative stress. *Mater Sci Eng C Mater Biol Appl*. 2021;123:111953. doi:10.1016/j.msec.2021.111953
11. Huang M, Liang C, Tan C, et al. Liposome co-encapsulation as a strategy for the delivery of curcumin and resveratrol. *Food Funct*. 2019;10:6447–6458. doi:10.1039/c9fo01338e
12. Liu F, Ma D, Luo X, et al. Fabrication and characterization of protein-phenolic conjugate nanoparticles for co-delivery of curcumin and resveratrol. *Food Hydrocolloid*. 2018;79:450–461. doi:10.1016/j.foodhyd.2018.01.017
13. Gonçalves A, Rocha F, Estevinho BN. Co-encapsulation of retinoic acid, curcumin and resveratrol by spray-drying of alginic acid sodium-based emulsions and ethyl cellulose-based solutions: impact on the co-delivery profiles. *Int J Biol Macromol*. 2023;224:1217–1227. doi:10.1016/j.ijbiomac.2022.10.207
14. Bohara RA, Tabassum N, Singh MP, et al. Recent overview of resveratrol's beneficial effects and its nano-delivery systems. *Molecules*. 2022;27(16):5154. doi:10.3390/molecules27165154
15. Rosales TKO, da Silva FF, Bernardes ES, et al. Plant-derived polyphenolic compounds: nanodelivery through polysaccharide-based systems to improve the biological properties. *Crit Rev Food Sci*. 2023:1–25. doi:10.1080/10408398.2023.2245038
16. Khan MA, Yue C, Fang Z, et al. Alginate/chitosan-coated zein nanoparticles for the delivery of resveratrol. *J Food Eng*. 2019;258:45–53. doi:10.1016/j.jfoodeng.2019.04.010
17. Li J, Ma J, Chen S, et al. Characterization of calcium alginate/ deacetylated konjac glucomannan blend films prepared by Ca^{2+} crosslinking and deacetylation. *Food Hydrocolloid*. 2018;82:363–369. doi:10.1016/j.foodhyd.2018.04.022
18. Fu X, Liu Z, Zhu C, et al. Nondigestible carbohydrates, butyrate, and butyrate-producing bacteria. *Crit Rev Food Sci*. 2019;59:S130–S152. doi:10.1080/10408398.2018.1542587
19. Zhang Z, Gu M, You X, et al. Encapsulation of bifidobacterium in alginate microgels improves viability and targeted gut release. *Food Hydrocolloid*. 2021;116:106634. doi:10.3390/molecules24071421
20. Han C, Fang L, Song S, et al. Polysaccharides-based delivery system for efficient encapsulation and controlled release of food-derived active peptides. *Carbohyd Polym*. 2022;291:119580. doi:10.1016/j.carbpol.2022.119580
21. Chen X, Wu YC, Gong PX, et al. Co-assembly of foxtail millet prolamin-lecithin/alginate sodium in citric acid-potassium phosphate buffer for delivery of quercetin. *Food Chem*. 2022;381:132268. doi:10.1016/j.foodchem.2022.132268
22. Wang L, Zhou Y, Wu M, et al. Functional nanocarrier for drug and gene delivery via local administration in mucosal tissues. *Nanomedicine*. 2018;13:69–88. doi:10.2217/nnm-2017-0143

23. Tie S, Tan M. Current advances in multifunctional nanocarriers based on marine polysaccharides for colon delivery of food polyphenols. *J Agric Food Chem*. 2022;70:903–915. doi:10.1021/acs.jafc.1c05012
24. Khalid S, Abbas G, Hanif M, et al. Thiolated sodium alginate conjugates for mucoadhesive and controlled release behavior of metformin microspheres. *Int J Biol Macromol*. 2020;164:2691–2700. doi:10.1016/j.ijbiomac.2020.08.116
25. Hou R, Chen J, Yue C, et al. Modification of lily polysaccharide by selenylation and the immune-enhancing activity. *Carbohyd Polym*. 2016;142:73–81. doi:10.1016/j.carbpol.2016.01.032
26. Li S, Sun W, Zhang K, et al. Selenium deficiency induces spleen pathological changes in pigs by decreasing selenoprotein expression, evoking oxidative stress, and activating inflammation and apoptosis. *J Anim Sci Biotechnol*. 2021;12:65. doi:10.1186/s40104-021-00587-x
27. Wang L, Li X, Wang B. Synthesis, characterization and antioxidant activity of selenium modified polysaccharides from Hohenbuehelia serotina. *Int J Biol Macromol*. 2018;120:1362–1368. doi:10.1016/j.ijbiomac.2018.09.139
28. Chen W, Cheng H, Xia W. Construction of polygonatum sibiricum polysaccharide functionalized selenium nanoparticles for the enhancement of stability and antioxidant activity. *Antioxidants Basel*. 2022;11(2):240. doi:10.3390/antiox11020240
29. Zhang X, Huo H, Sun X, et al. Nanocrystallization of anthocyanin extract from red-fleshed apple "QN-5" improved its antioxidant effect through enhanced stability and activity under stressful conditions. *Molecules*. 2019;24:1421. doi:10.3390/molecules24071421
30. Fan L, Lin L, Zhang Y, et al. Component characteristics and reactive oxygen species scavenging activity of anthocyanins from fruits of Lonicera caerulea L. *Food Chem*. 2023;403:134391. doi:10.1016/j.foodchem.2022.134391
31. Teng C, Qin P, Shi Z, et al. Structural characterization and antioxidant activity of alkali-extracted polysaccharides from quinoa. *Food Hydrocolloid*. 2021;113:105392. doi:10.1016/j.foodhyd.2020.106392
32. Wei Z, Fan Z, Peng G, et al. Extracorporeal hemoperfusion therapy for sepsis: multi-lamellar microspheres towards cascade endotoxin removal and broad-spectrum radical eliminating. *Chem Eng J*. 2022;444:136499. doi:10.1016/j.cej.2022.136499
33. Huang X, Liu Y, Zou Y, et al. Encapsulation of resveratrol in zein/pectin core-shell nanoparticles: stability, bioaccessibility, and antioxidant capacity after simulated gastrointestinal digestion. *Food Hydrocolloid*. 2019;93:261–269. doi:10.1016/j.foodhyd.2019.02.039
34. Kafedjiiski K, Krauland AH, Hoffer MH, et al. Synthesis and in vitro evaluation of a novel thiolated chitosan. *Biomaterials*. 2005;26:819–826. doi:10.1016/j.biomaterials.2004.03.011
35. Chivangkul T, Pengprecha S, Padungros P, et al. Enhanced water-solubility and mucoadhesion of N,N,N-trimethyl-N-gluconate-N-homocysteine thiolactone chitosan. *Carbohyd Polym*. 2014;108:224–231. doi:10.1016/j.carbpol.2014.02.078
36. Chen W, Rezaizadehnajafi L, Wink M. Influence of resveratrol on oxidative stress resistance and life span in Caenorhabditis elegans. *J Pharm Pharmacol*. 2013;65:682–688. doi:10.1111/jphp.12023
37. Duhon SA, Murakami S, Johnson TEGD. Direct isolation of longevity mutants in the nematode Caenorhabditis elegans. *Dev Genet*. 1996;8:144–153. doi:10.1002/(sici)1520-6408(1996)18:2<144::aid-dvg7>3.0.co;2-9
38. Li Q, Zhu L, Qi X, et al. Immunostimulatory and antioxidant activities of the selenized polysaccharide from edible Grifola frondosa. *Food Sci Nutr*. 2022;10:1289–1298. doi:10.1002/fsn3.2764
39. Kotla NG, Singh R, Baby BV, et al. Inflammation-specific targeted carriers for local drug delivery to inflammatory bowel disease. *Biomaterials*. 2022;281:121364. doi:10.1016/j.biomaterials.2022.121364
40. Cho AR, Chun YG, Kim BK, et al. Preparation of chitosan-TPP microspheres as resveratrol carriers. *J Food Sci*. 2014;79(4):568–576. doi:10.1111/1750-3841.12395
41. Jensen M, Kierulf-Vieira W, Kooyman PJ, et al. Variable temperature in situ TEM mapping of the thermodynamically stable element distribution in bimetallic Pt–Rh nanoparticles. *Nanoscale Adv*. 2023;5:5286–5294. doi:10.1039/d3na00448a
42. Tian B, Liu J. Resveratrol: a review of plant sources, synthesis, stability, modification and food application. *J Sci Food Agr*. 2019;100:1392–1404. doi:10.1002/jsfa.10152
43. Shankar SK, Praveen Kumar SK, Mulimani VH. Calcium alginate entrapped preparation of α-galactosidase: its stability and application in hydrolysis of soymilk galactooligosaccharides. *J Ind Microbiol Biot*. 2010;38:1399–1405. doi:10.1007/s10295-010-0925-0
44. Xu T, Gu Z, Cheng L, et al. Stability, oxidizability, and topical delivery of resveratrol encapsulated in octenyl succinic anhydride starch/chitosan complex-stabilized high internal phase Pickering emulsions. *Carbohyd Polym*. 2023;305:120566. doi:10.1016/j.carbpol.2023.120566
45. Zhang Z, Yan A, Xu Z, et al. Engineering biomimetic ATP-responsive Se-containing core-shell cascade nanozyme for efficient tumor combination therapy. *Chem Eng J*. 2023;454:140165. doi:10.1016/j.cej.2022.140165
46. Korkut OÇ, Özdemir G. Encapsulation of resveratrol in rhamnolipid-zein nanoparticles using a pH-driven method: kinetic modeling on controlled release from nanoparticles. *J Disper Sci Technol*. 2023;1–11. doi:10.1080/01932691.2023.2197044
47. Bai -L-L, Zhang L-Q, Ma J, et al. DIP2A is involved in SOD-mediated antioxidative reactions in murine brain. *Free Radical Bio Med*. 2021;168:6–15. doi:10.1016/j.freeradbiomed.2021.03.027
48. Sayed AEDH, Mohamed NH, Ismail MA, et al. Antioxidant and antiapoptotic activities of Calotropis procera latex on Catfish (Clarias gariepinus) exposed to toxic 4-nonylphenol. *Ecotox Environ Safe*. 2016;128:189–194. doi:10.1016/j.ecoenv.2016.02.023
49. Zhang Y, Zhu S, Wang X, et al. The effect of dietary selenium levels on growth performance, antioxidant capacity and glutathione peroxidase 1 (GSHPx1) mRNA expression in growing meat rabbits. *Anim Feed Sci Tech*. 2011;169:259–264. doi:10.1016/j.anifeedsci.2011.07.006
50. Dues DJ, Schaar CE, Johnson BK, et al. Uncoupling of oxidative stress resistance and lifespan in long-lived isp-1 mitochondrial mutants in Caenorhabditis elegans. *Free Radical Bio Med*. 2017;108:362–373. doi:10.1016/j.freeradbiomed.2017.04.004
51. Silva RC, Teixeira JA, Nunes WDG, et al. Resveratrol: a thermoanalytical study. *Food Chem*. 2017;237:561–565. doi:10.1016/j.foodchem.2017.05.146
52. Mi X-N, Wang L-F, Hu Y, et al. Methyl 3,4-dihydroxybenzoate enhances resistance to oxidative stressors and lifespan in *C. elegans* partially via daf-2/daf-16. *Int J Mol Sci*. 2018;19(6):1670. doi:10.3390/ijms19061670